

---

# Constraining cosmological parameters from N-body simulations with Variational Bayesian Neural Networks

Héctor J. Hortúa<sup>1,2,\*</sup>, Luz Ángela García<sup>3</sup> and Leonardo Castañeda C.<sup>4</sup>

<sup>1</sup> *Grupo Signos, Departamento de Matemáticas, Universidad el Bosque, Bogotá, Colombia.*

<sup>2</sup> *Maestría en Ciencia de Datos, Universidad Escuela Colombiana de Ingeniería Julio Garavito Bogotá, Colombia.*

<sup>3</sup> *Universidad ECCI. Cra. 19 No. 49-20, Bogotá, Colombia, Código Postal 111311.*

<sup>4</sup> *Observatorio Astronómico Nacional, Universidad Nacional de Colombia, Bogotá, Colombia.*

Correspondence\*:

-  
hjhortuao@unal.edu.co

## ABSTRACT

Methods based on Deep Learning have recently applied on astrophysical parameter recovery thanks to their ability to capture information from complex data. One of these methods are the approximate Bayesian Neural Networks (BNNs) which have demonstrated to yield consistent posterior distribution into the parameter space, helpful for uncertainty quantification. However, as any modern neural networks, they tend to produce overly confident uncertainty estimates, and can introduce bias when BNNs are applied to data. In this work, we implement multiplicative normalizing flows (MNFs), a family of approximate posteriors for the parameters of BNNs with the purpose of enhancing the flexibility of the variational posterior distribution, to extract  $\Omega_m$ ,  $h$ , and  $\sigma_8$  from the QUIJOTE simulations. We have compared this method with respect to the standard BNNs, and the flipout estimator. We found that MNFs combined with BNNs outperform the other models obtaining predictive performance with almost one order of magnitude larger than standard BNNs,  $\sigma_8$  extracted with high accuracy ( $r^2 = 0.99$ ), and precise uncertainty estimates. The latter implies that MNFs provide more realistic predictive distribution closer to the true posterior mitigating the bias introduced by the variational approximation, and allowing to work with well calibrated networks.

**Keywords:** cosmology, N-body simulations, parameter estimation, artificial intelligence, deep neural networks

## 1 INTRODUCTION

Cosmological simulations offer one of the most powerful ways to understand the initial conditions of the Universe and improve our knowledge on fundamental physics (1). They open also the possibility to fully explore the growth of structure in both the linear and non-linear regime. Currently, the concordance cosmological model,  $\Lambda$ -CDM, gives an accurate description of most of the observations from early to late stages of the Universe using a set of few parameters (2). Recent observations from Cosmic Microwave Background (CMB) have provided such accurate estimation for the cosmological parameters, and prompted a tension with respect to local scales measurement, along with a well-known degeneracy on the total non-relativistic matter density parameters (3, 4, 5). Conventionally, the way to capture information from

astronomical observations is to compare summary statistics from data against theory predictions. However, two major difficulties arise: First, it is not well understood what kind of estimator, or at which degree of approximation of order statistic should be better to extract the maximum information from observations. In fact, the most common choice is the power spectrum(PS) which has shown to be a powerful tool for making inference (2). However, It is well known that PS is not able to fully characterize the statistical properties of non-Gaussian density fields, yielding that it would not be suitable for upcoming Large Scale Structure (LSS) or 21-cm signals which are highly non-Gaussian (6, 7, 8). Then, PS will miss relevant information if only this statistic is used for parameter recovery (9). Second, Cosmologists will require to store and process a large number of data, which can be very expensive. Clearly, sophisticated computational tools along with new perspectives on data collection, storage, and analysis must be developed in order to interpret these observations (10).

In recent years, artificial intelligence (AI), and Deep Neural Networks (DNNs) have emerged as promising tools to tackle the aforementioned difficulties in the cosmological context due to its capability for learning relationships between variables in complex data, outperform traditional estimators, and handle the demanding computational needs in Astrophysics and Cosmology (10). These standard DNNs have been used on a variety of tasks because of their potential for solving inverse problems. However, they are prone to overfitting due to the excessive number of parameters to be adjusted, and the lack of explanations of their predictions for given instances (11). The latter is crucial for cosmological analysis where assessing robustness and reliability of the model predictions are imperative. This problem can be addressed by endowing DNNs with probabilistic properties that permit quantifying posterior distributions on their outcomes, and provide them with predictive uncertainties. One of these approaches is the use of Bayesian Neural Networks (BNNs) comprised of probabilistic layers that capture uncertainty over the network parameters (weights), and trained using Bayesian inference (12). Several works have utilized BNNs in cosmological scenarios where the combination of DNNs (through Convolutional Neural Networks, CNNs) and probabilistic properties, allow to build models adapted to non-Gaussian data without requiring a priori choice summary statistic (9, 13, 14, 15), along with quantifying predictive uncertainties (16, 17, 18, 19, 20, 21). Indeed, BNNs permit to infer posterior distributions instead of point estimates for the weights. These distributions capture the parameter uncertainty, and by subsequently integrating over them, we acquire uncertainties related to the network outputs. Nevertheless, obtaining the posterior distributions is an intractable task, and approximate techniques such as a Variational Inference(VI) must be used in order to put them into practice (22). Despite the approximate posterior distribution over the weights employed in VI clearly providing fast computations for inference tasks, they can also introduce a degree of bias depending on how complex(or simple) the choice of the approximate distribution family is (23). This issue yields overconfident uncertainty predictions and an unsatisfactory closeness measurement with respect to the true posterior. In (17, 18), the authors included normalizing flows on the top of BNNs to give the joint parameter distribution more flexibility. However, that approach is not implemented into the Bayesian framework, preserving the bias.

In this paper, we attempt to enhance the flexibility of the approximate posterior distribution over the weights of the network by employing multiplicative normalizing flows, resulting in accurate and precise uncertainty estimates provided by BNNs. We apply this approach to N-body simulations taken from QUIJOTE dataset (24) in order to show how BNNs can take not only advantage of non-Gaussian signals without requiring a specifying the summary statistic (such as PS) but also, increase the posterior complexity, as they yield much larger performance improvements. This paper is organized as follows. Section 2 offers a summary of the BNNs framework and a detailed description of Normalizing flow implementation. Section 3 describes the dataset and analysis tools used in this paper. Numerical implementation and configuration for

BNNs are described in Section 4. Section 5 presents the results we obtained by training BNNs taking into account different approaches and we display the inference of cosmological parameters. It also outlines the calibration diagrams to determine the accuracy of the uncertainty estimates. Finally, Section 6 draws the main conclusions of this work and possible further directions to the use of BNNs in Cosmology.

## 2 VARIATIONAL BAYESIAN NEURAL NETWORKS

Here we go into detail about Bayesian Neural Networks (BNNs), and their implementation to perform parameter inference. We start with a brief introduction, before focusing on improving the variational approximation. We remind the reader to refer to (25, 26, 22) for further details.

### 2.1 Approximate BNNs

The goal of BNNs is to infer the posterior distribution  $p(w|\mathcal{D})$  over the weights  $w$  of the network after observing the data  $\mathcal{D} = (X, Y)$ . This posterior can be obtained from Bayes law:  $p(w|\mathcal{D}) \sim p(\mathcal{D}|w)p(w)$ , given a likelihood function  $p(\mathcal{D}|w)$ , and a prior on the weights  $p(w)$ . Once the posterior has been computed, the probability distribution on a new test example  $x^*$  is given by

$$p(y^*|x^*, \mathcal{D}) = \int_w p(y^*|x^*, w)p(w|\mathcal{D})dw, \quad (1)$$

where  $p(y^*|x^*, w)$  is the predictive distribution for a given value of the weights. For neural networks, however, computing the exact posterior is intractable, so one must resort to approximate BNNs for inference (26). A popular method to approximate the posterior is variational inference (VI) (22). Let  $q(w|\theta)$  be a family of simple distributions parameterized by  $\theta$ . So, the goal of VI is to select a distribution  $q(w|\theta^*)$  such that  $\theta^*$  minimizes  $KL[q(w|\theta)||p(w|\mathcal{D})]$ , being  $KL[\cdot||\cdot]$  the Kullback-Leibler divergence. This minimization is equivalent to maximizing the evidence lower bound (ELBO) (26)

$$\text{ELBO}(\theta) = \mathbb{E}_{q(w|\theta)}[\log p(Y|X, w)] - \text{KL}[q(w|\theta)||p(w)], \quad (2)$$

where  $\mathbb{E}_{q(w|\theta)}[\log p(Y|X, w)]$  is the expected log-likelihood with respect to the variational posterior and  $\text{KL}[q(w|\theta)||p(w)]$  is the divergence of the variational posterior from the prior. We can observe from Eq. 2 that the KL divergence acts as a regularizer that encourages the variational posterior moves towards the modes of the prior. A common choice for the variational posterior is a product of independent (i.e., mean-field) Gaussian distributions, one distribution for each parameter  $w$  in the network (25)

$$q(w|\theta) = \prod_{ij} \mathcal{N}(w; \mu_{ij}, \sigma_{ij}^2) \quad (3)$$

being  $i$  and  $j$  the indices of the neurons from the previous layer and the current layer respectively. Applying the reparametrization trick we arrive at  $w_{ij} = \mu_{ij} + \sigma_{ij} * \epsilon_{ij}$ , where  $\epsilon_{ij}$  is drawn from a standard normal distribution. Furthermore, if the prior is also a product of independent Gaussians, the KL divergence between the prior and the variational posterior be computed analytically, which makes this approach computationally efficient.

#### 2.1.1 Flipout

In case where sampling from  $q(w|\theta)$  is not fully independently for different examples in a mini-batch, we will obtain gradient estimates with high variance. Flipout method provides an alternative to decorrelate the

gradients within a mini batch by implicitly sampling pseudo-independent weights for each example (27). The method requires two assumptions about the properties of  $q(w|\theta)$ : symmetric with respect to zero, and the weights of the network are independent. Under these assumptions, the distribution is invariant to element wise multiplication by a random sign matrix  $\hat{r}$ , i.e.,  $\hat{w} = w \circ \hat{r}$ , implies that  $w \sim q(w) \approx \hat{w} \sim \hat{q}(\hat{w})$ . Therefore, the marginal distribution over gradients computed for individual examples will be identical to the distribution computed using shared weights samples. Hence, Flipout achieves much lower variance updates when averaging over a mini batch. We validate this approach experimentally by comparing against Multiplicative normalizing flows.

## 2.2 Uncertainty in BNNs

BNNs offer a groundwork to incorporate from the posterior distribution both, the uncertainty inherent to the data (aleatoric uncertainty), and the uncertainty in the model parameters due to a limited amount of training data (epistemic uncertainty) (28). Following (16), assuming that the top of the BNNs consist of a mean vector  $\mu \in \mathbb{R}^N$  and a covariance matrix  $\Sigma \in \mathbb{R}^{N(N+1)/2}$ , and for a given fixed input  $x^*$ ,  $T$  forward passes of the network are computed, obtaining for each of their mean  $\mu_t$  and covariance matrix  $\Sigma_t$ . Then, an estimator for approximate the predictive covariance can be written as

$$\widehat{\text{Cov}}(y^*, y^* | x^*) \approx \underbrace{\frac{1}{T} \sum_{t=1}^T \Sigma_t}_{\text{Aleatoric}} + \underbrace{\frac{1}{T} \sum_{t=1}^T (\mu_t - \bar{\mu})(\mu_t - \bar{\mu})^T}_{\text{Epistemic}}, \quad (4)$$

with  $\bar{\mu} = \frac{1}{T} \sum_{t=1}^T \mu_t$ . Notice that in case  $\Sigma$  is diagonal, and  $\sigma^2 = \text{diag}(\Sigma)$ , the last equation reduces to the results obtained in (29, 30)

$$\widehat{\text{Var}}(y^* | x^*) \approx \underbrace{\frac{1}{T} \sum_{t=1}^T \sigma_t^2}_{\text{Aleatoric}} + \underbrace{\frac{1}{T} \sum_{t=1}^T (\mu_t - \bar{\mu})^2}_{\text{Epistemic}}. \quad (5)$$

In this scenario, BNNs can be used to learn the correlations between the the targets and produce estimates of their uncertainties. Unfortunately, the uncertainty computed from Eqs. 4, 5, tends to be miscalibrated, i.e., the predicted uncertainty (taking into account both epistemic and aleatoric uncertainty) is underestimated and does not allow robust detection of uncertain predictions at inference. Therefore, calibration diagrams along with methods to jointly calibrate aleatoric and epistemic uncertainties, must be employed before inferring predictions from BNNs (31). We come back to this point in Section 5.

## 2.3 Multiplicative normalizing flows

As mentioned previously, the most common family for the variational posterior used in BNNs is the mean-field Gaussian distributions defined in Eq. 3. This simple distribution is unable to capture the complexity of the true posterior. Therefore, we expect that increasing the complexity of the variational posterior, BNNs achieve significant performance gains since we are now able to sample from a complicate distribution that more closely resembles the true posterior. Certainly, transforming the variational posterior must be followed with fast computations and still being numerically tractable. We now describe in detail the Multiplicative Normalizing Flows (MNFs) method that provides flexible posterior distributions in an

<sup>1</sup> Where the targets  $y \in \mathbb{R}^N$ .

efficient way by employing auxiliary random variables and normalizing flows proposed by (32). MNFs propose that the variational posterior can be expressed as an infinite mixture of distributions

$$q(w|\theta) = \int q(w|z, \theta)q(z|\theta)dz \quad (6)$$

where  $\theta$  is the learnable posterior parameter, and  $z \sim q(z|\theta) \equiv q(z)^2$  is a vector with the same dimension on the input layer, which plays the role of an auxiliary latent variable. Moreover, allowing local reparametrizations, the variational posterior for fully connected layers become a modification of Eq. 3 written as

$$w \sim q(w|z) = \prod_{ij} \mathcal{N}(w; z_i \mu_{ij}, \sigma_{ij}^2). \quad (7)$$

Notice that by enhancing the complexity of  $q(z)$ , we can increase the flexibility of the variational posterior. This can be done using Normalizing Flows since the dimensionality of  $z$  is much lower compared to the weights. Starting from samples  $z_0 \sim q(z_0)$  from fully factorized Gaussian Eq. 3, a rich distribution  $q(z_K)$  can be obtained by applying a successively invertible  $K$ -transformations  $f_K$  on  $z_0$

$$z_K = \text{NF}(z_0) = f_K \circ \dots \circ f_1(z_0); \quad \log q(z_K) = \log q(z_0) - \sum_{k=1}^K \log \left| \det \frac{\partial f_k}{\partial z_{k-1}} \right|. \quad (8)$$

Unfortunately, the KL divergence in Eq. 2 becomes generally intractable as the posterior  $q(w)$  is an infinite mixture as shown in Eq. 6. This is addressed also in (33) by evoking Bayes law  $q(z_K)q(w|z_K) = q(w)q(z_K|w)$  and introducing an auxiliary distribution  $r(z_K|w, \phi)$  parameterized by  $\phi$ , with the purpose of approximating the posterior distribution of the original variational parameters  $q(z_K|w)$  to further lower bound the KL divergence term. Therefore, KL divergence term can be bounded as follows

$$\begin{aligned} -\text{KL} [q(w)||p(w)] &= -\mathbb{E}_{q(w)} \left[ \log \left( \frac{q(w)}{p(w)} \right) \right] \\ &\geq -\mathbb{E}_{q(w)} \left[ \log \left( \frac{q(w)}{p(w)} \right) + \text{KL} [q(z_K|w)||r(z_K|w, \phi)] \right] \\ &= -\mathbb{E}_{q(w)} \left[ \log \left( \frac{q(w)}{p(w)} \right) + \mathbb{E}_{q(z_K|w)} \left[ \log \left( \frac{q(z_K|w)}{r(z_K|w, \phi)} \right) \right] \right] \\ &= -\mathbb{E}_{q(w)} \left[ \mathbb{E}_{q(z_K|w)} \left[ \log \left( \frac{q(w)}{p(w)} \right) \right] + \mathbb{E}_{q(z_K|w)} \left[ \log \left( \frac{q(z_K|w)}{r(z_K|w, \phi)} \right) \right] \right] \quad (9) \\ &= -\mathbb{E}_{q(w, z_K)} \left[ \log \left( \frac{q(w)}{p(w)} \right) + \log \left( \frac{q(z_K|w)}{r(z_K|w, \phi)} \right) \right] \\ &= \mathbb{E}_{q(w, z_K)} [-\log (q(w)q(z_K|w)) + \log r(z_K|w, \phi) + \log p(w)] \Rightarrow \\ -\text{KL} [q(w)||p(w)] &\geq \mathbb{E}_{q(w, z_K)} [-\text{KL} [q(w|z_K)||p(w)] + \log q(z_K) + \log r(z_K|w, \phi)], \end{aligned}$$

where we have taken into account that  $\text{KL}[P||Q] \geq 0$ , and the equality is satisfied iff  $P = Q$ . In the last line, the first term can be analytically computed since it will be the KL divergence between two Gaussian distributions, while the second term is given by the Normalizing flow generated by  $f_K$  as we observe in

<sup>2</sup> The parameter  $\theta$  will be omitted in this section for clarity of notation.

Eq. 8. Finally, the auxiliary posterior term is parameterized by inverse normalizing flows as follows (34)

$$z_0 = \text{NF}^{-1}(z_K) = g_1^{-1} \circ \dots \circ g_K^{-1}(z_K); \quad \log r(z_K|w, \phi) = \log r(z_0|w, \phi) + \sum_{k=1}^K \log \left| \det \frac{\partial g_k^{-1}}{\partial z_k} \right|, \quad (10)$$

where one can parameterize  $g_K^{-1}$  as another normalizing flow. In the paper (32), the authors also propose a flexible parametrization of the auxiliary posterior as

$$z_0 \sim r(z_K|w, \phi) = \prod_i \mathcal{N}(z_0; \tilde{\mu}_i(w, \phi), \tilde{\sigma}_i^2(w, \phi)). \quad (11)$$

We will use the parameterization of the mean  $\tilde{\mu}$ , and the variance  $\tilde{\sigma}^2$  as in the original paper as well as the masked RealNVP (35) as choice of Normalizing flows.

### 3 N-BODY SIMULATIONS DATASET

In this work, we leverage 2000 hypercubes simulation taken from The Quijote project (24). They have been run using the TreePM code Gadget-III (36), and their initial conditions were generated at  $z = 127$  using 2LPT (37). The set chosen for this work is made of standard simulations with different random seeds with the intention of emulating the cosmic variance. Each instance corresponds to a three-dimensional distribution of the density field with size  $64^3$ . The cosmological parameters vary according to  $\Omega_m \in [0.1, 0.5]$ ,  $\Omega_b \in [0.03, 0.07]$ ,  $h \in [0.5, 0.9]$ ,  $n_s \in [0.8, 1.2]$ ,  $\sigma_8 \in [0.6, 1.0]$ , while neutrino mass ( $M_\nu = 0\text{eV}$ ) and the equation of state parameter ( $w = -1$ ) are kept fixed. The dataset was split into training (70%), validation (10%), and test (20%), while hypercubes were logarithmic transformed and the cosmological parameters normalized between 0 and 1. In this paper we will build BNNs with the ability to predict three out of five aforementioned parameters,  $\Omega_m$ ,  $\sigma_8$  and  $h$ .

### 4 BNNs IMPLEMENTATION

We will consider three different BNNs architectures based on the discussion presented in Section 2: standard BNNs (prior and variational posterior defined as a mean-field Normal distributions) [**sBNNs**]; BNNs with Flipout estimator [**FlipoutBNNs**]; and Multiplicative normalizing flows [**VBNNs**]. The experiments were implemented using the TensorFlow v:2.9 and TensorFlow-probability v:0.19 (38). All BNNs designed in this paper are comprised of three parts. First, all experiments start with a  $64^3$ -voxel input layer corresponding to the normalised 3D density field followed by the fully-convolutional ResNet-18 backbone as it is presented schematically in table 1. All the Resblock are fully pre-activated and their representation can be seen in figure. 1. The repository Classification models 3D was used to build the backbone of BNNs (39). Subsequently, the second part of BNNs represents the stochasticity of the network. This is comprised of just one layer and it depends on the type of BNN used. For *sBNNs*, we employ the dense variational layer which uses variational inference to fit an approximate posterior to the distribution over both the kernel matrix and the bias terms. Here, we use as posterior and prior (no-trainable) Normal distributions. Experiments with *FlipoutBNNs* for instance, are made via Flipout dense layer where the mean field normal distribution are also utilized to parameterize the distributions. These two layers are already implemented in the package TF-probability (38). On the other hand, for VBNNs we have adapted the class DenseMNF implemented in the repositories TF-MNF, MNF-VBNN (32) to our model. Here, we use 50 layers for the masked RealNVP NF, and the maximum variance for layer weights is around the unity. Finally, the last

ResNet-18 backbone		
Layer Name	Input Shape	Output Shape
Batch Norm	$(N_{\text{batch}}, 64, 64, 64, 3)$	$(N_{\text{batch}}, 64, 64, 64, 3)$
3D Convolutional	$(N_{\text{batch}}, 70, 70, 70, 3)$	$(N_{\text{batch}}, 32, 32, 32, 64)$
Batch Norm+ReLU	$(N_{\text{batch}}, 32, 32, 32, 64)$	$(N_{\text{batch}}, 32, 32, 32, 64)$
Max Pooling 3D	$(N_{\text{batch}}, 34, 34, 34, 64)$	$(N_{\text{batch}}, 16, 16, 16, 64)$
Batch Norm+ReLU	$(N_{\text{batch}}, 16, 16, 16, 64)$	$(N_{\text{batch}}, 16, 16, 16, 64)$
Resblock 1	$\begin{bmatrix} (N_{\text{batch}}, 16, 16, 16, 64) \\ (N_{\text{batch}}, 16, 16, 16, 64) \end{bmatrix}$	$(N_{\text{batch}}, 16, 16, 16, 64)$
Batch Norm+ReLU	$(N_{\text{batch}}, 16, 16, 16, 64)$	$(N_{\text{batch}}, 16, 16, 16, 64)$
Resblock 2	$\begin{bmatrix} (N_{\text{batch}}, 16, 16, 16, 64) \\ (N_{\text{batch}}, 8, 8, 8, 128) \end{bmatrix}$	$(N_{\text{batch}}, 8, 8, 8, 128)$
Batch Norm+ReLU	$(N_{\text{batch}}, 8, 8, 8, 128)$	$(N_{\text{batch}}, 8, 8, 8, 128)$
Resblock 3	$\begin{bmatrix} (N_{\text{batch}}, 8, 8, 8, 128) \\ (N_{\text{batch}}, 4, 4, 4, 256) \end{bmatrix}$	$(N_{\text{batch}}, 4, 4, 4, 256)$
Batch Norm+ReLU	$(N_{\text{batch}}, 4, 4, 4, 256)$	$(N_{\text{batch}}, 4, 4, 4, 256)$
Resblock 4	$\begin{bmatrix} (N_{\text{batch}}, 4, 4, 4, 256) \\ (N_{\text{batch}}, 2, 2, 2, 512) \end{bmatrix}$	$(N_{\text{batch}}, 2, 2, 2, 512)$
Batch Norm+ReLU	$(N_{\text{batch}}, 2, 2, 2, 512)$	$(N_{\text{batch}}, 2, 2, 2, 512)$
Global Avg Pooling	$(N_{\text{batch}}, 2, 2, 2, 512)$	$(N_{\text{batch}}, 512)$

**Table 1.** Configuration of the backbone BNNs used for all experiments presented in this paper.

part of all BNNs account for the output of the network, which is dependent on the aleatoric uncertainty parameterization. We use a 3D multivariate Gaussian distribution with nine parameters to be learnt (three means  $\mu$  for the cosmological parameters, and six elements for the covariance matrix  $\Sigma$ ).

The loss function to be optimized during training is given by the ELBO 2 where the second term is associated to the negative log-likelihood (NLL)

$$- \text{NLL} \sim \frac{1}{2} \log |s \cdot \Sigma| + \frac{1}{2} (\mathbf{y} - \mu)^\top (s \cdot \Sigma)^{-1} (\mathbf{y} - \mu), \quad (12)$$

averaged over the mini-batch. The scalar variable  $s$  is equal to one during the training process, and it becomes a trainable variable during post-training to recalibrate the probability density function (16, 31). The algorithm used to minimize the objective function is the Adam optimizer with first and second moment exponential decay rates of 0.9 and 0.999, respectively (40). The learning rate starts from  $10^{-3}$  and it will be reduced by a factor of 0.8 in case that any improvement has not been observed after 10 epochs. Furthermore, we have applied warm-up period for which the model turns on progressively the KL term in Eq. 2. This is achieved by introducing a  $\beta$  variable in the ELBO, i.e.,  $\beta \cdot \text{KL} [q(w|\theta) || p(w)]$ , so, this parameter starts being equal to 0 and grows linearly to 1 during 10 epochs (41). BNNs were trained with 32 batches and early stopping callback for avoiding over-fitting. The infrastructure used was the Google Cloud Platform (GCP) using a nvidia-tesla-t4 of 16 GB GDDR6 in a N1 machine series shared-core.

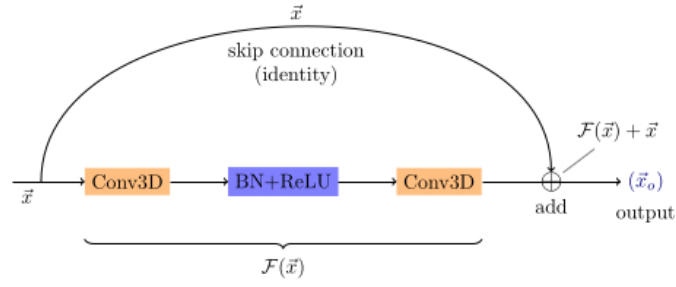


**Figure 1a.** Illustration of the first skip connection in a residual block.

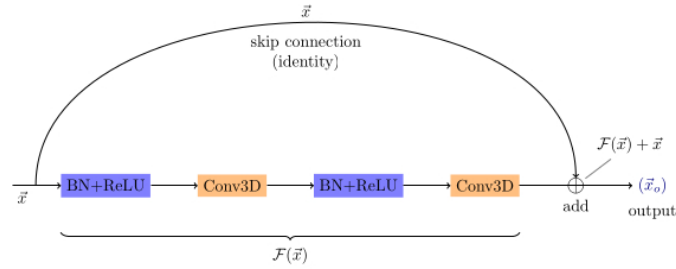


**Figure 1b.** Illustration of the second skip connection in the residual block.

**Figure 1.** Each Resblock includes both skip connection configurations. **(A)** The Resblock starts with this configuration applied to the input tensor. **(B)** The output of the previous configuration is fed into this connection.

#### 4.1 Metrics

We compare all BNN results in terms of performance, i.e., the precision of their predictions for the cosmological parameters quantified through Mean Square Error (MSE), ELBO, and plotting the true vs predicted values with its coefficient of determination. Also, it is important to quantify the quality of the uncertainty estimates. One of the ways to diagnostic the quality of the uncertainty estimates is through reliability diagrams. Following (31, 11), we can define perfect calibration of regression uncertainty as

$$\mathbb{E}_{\hat{\sigma}^2} [ |(\mathbb{E}[(\mathbf{y} - \boldsymbol{\mu})^2] | \hat{\sigma}^2 = \alpha^2) - \alpha^2| ] \quad \forall \{ \alpha^2 \in \mathbb{R} \mid \alpha^2 \geq 0 \}. \quad (13)$$

Hence, the predicted uncertainty  $\hat{\sigma}^2$  is partitioned into  $K$  bins with equal width, and the variance per bin is defined as

$$\text{var}(B_k) := \frac{1}{|B_k|} \sum_{i \in B_k} \frac{1}{N} \sum_{n=1}^N (\boldsymbol{\mu}_{i,n} - \mathbf{y}_i)^2, \quad (14)$$

with  $N$  stochastic forward passes. On the other hand, the uncertainty per bin is defined as

$$\text{uncert}(B_k) := \frac{1}{|B_k|} \sum_{i \in B_k} \hat{\sigma}_i^2. \quad (15)$$

With these two quantities, we can generate reliability diagrams to assess the quality of the estimated uncertainty via plotting  $\text{var}(B_k)$  vs.  $\text{uncert}(B_k)$ . In addition, we can compute the expected uncertainty



Metrics	FlipoutBNNs					VBNNs					sBNNs				
	$\Omega_m$	$\sigma_8$	$h$	$\Omega_m h^2$	$\sigma_8 \Omega_m^{0.25}$	$\Omega_m$	$\sigma_8$	$h$	$\Omega_m h^2$	$\sigma_8 \Omega_m^{0.25}$	$\Omega_m$	$\sigma_8$	$h$	$\Omega_m h^2$	$\sigma_8 \Omega_m^{0.25}$
MSE	0.063					0.057					0.190				
ELBO	20.85					19.71					31.57				
$r^2$	0.82	0.98	0.2	0.03	0.93	0.85	0.99	0.4	0.56	0.95	0.75	0.85	0.01	0.23	0.80
UCE	0.109	8.10	0.26			0.0008	0.0008	0.010			>1.0				

**Table 2.** Metrics test set results for all BNNs architectures. High UCE values indicate miscalibration. MSE and ELBO are computed only over the cosmological parameters.

calibration error (UCE) in order to quantify the miscalibration

$$\text{UCE} := \sum_{k=1}^K \frac{|B_k|}{m} |\text{var}(B_k) - \text{uncert}(B_k)|, \quad (16)$$

with number of inputs  $m$  and set of indices  $B_k$  of inputs, for which the uncertainty falls into the bin  $k$ . A more general approach proposed in (16) consists in computing the expected coverage probabilities defined as the  $x\%$  of samples for which the true value of the parameters falls in the  $x\%$ -confidence region defined by the joint posterior. Clearly, this option is more precise since it captures higher-order statistics through the full posterior distribution. However, for simplicity, we will follow the UCE approach.

## 5 ANALYSIS AND RESULTS OF PARAMETER INFERENCE WITH BNNs

In this section we discuss the results obtained by comparing three different versions of BNNs, the one with MNFs, the standard BNN, and the third one using Flipout as estimator. The results reported in this section were computed on the Test dataset. Table 2. shows the metrics obtained for each BNN approach. As mentioned, MSE, ELBO and  $r^2$  provide well estimates for determining the precision of the model, while UCE measures the miscalibration. Here, we can observe that VBNNs outperform all experiments, not only taking into account the average error, but also the precision for each cosmological parameter along with a good calibration in its uncertainty predictions. Followed by VBNNs, we have the FlipoutBNNs, however, although this approach yields good cosmological parameter estimation, it underestimates their uncertainties. Therefore, VBNNs avoids indeed the application of an extra post training step in the Machine Learning pipeline related to calibration. Notice that in all experiments,  $h$  becomes hardly predicted for all model. Figure 2 displays the predicted against true values for  $\Omega_m$ ,  $\omega_m$  (instead of  $h$ ),  $\sigma_8$  and the degeneracy direction defined as  $\sigma_8 \Omega_m^{0.25}$ . Error bars report the epistemic plus aleatoric uncertainties predicted by BNNs, which illustrates the advantages of these probabilistic models where the certainty prediction of the model is captured instead of traditional DNNs where only point estimates are present. This uncertainty was taken from the diagonal part of the covariance matrix.

### 5.1 Calibration metrics

In figure 3, we analyze the quality of our uncertainty measurement using calibration diagrams. We show the predicted uncertainty vs observed uncertainty from our model on the Test dataset. Better performing uncertainty estimates should correlate more accurately with the dashed lines. We can see that estimating uncertainty from VBNNs reflect better the real uncertainty. Furthermore, the scale for VBNNs is two orders of magnitude lower than FlipoutBNN, which also implies how reliable is this models according to their predictions. Notice that the even if we partitioned the variance into  $K = 10$  bins with equal width, FlipoutBNNs and sBNNs yield underestimate uncertainties (many examples concentrates in lower bin values), for this reason we see that while VBNNs supply all ten samples in the calibration plots, for

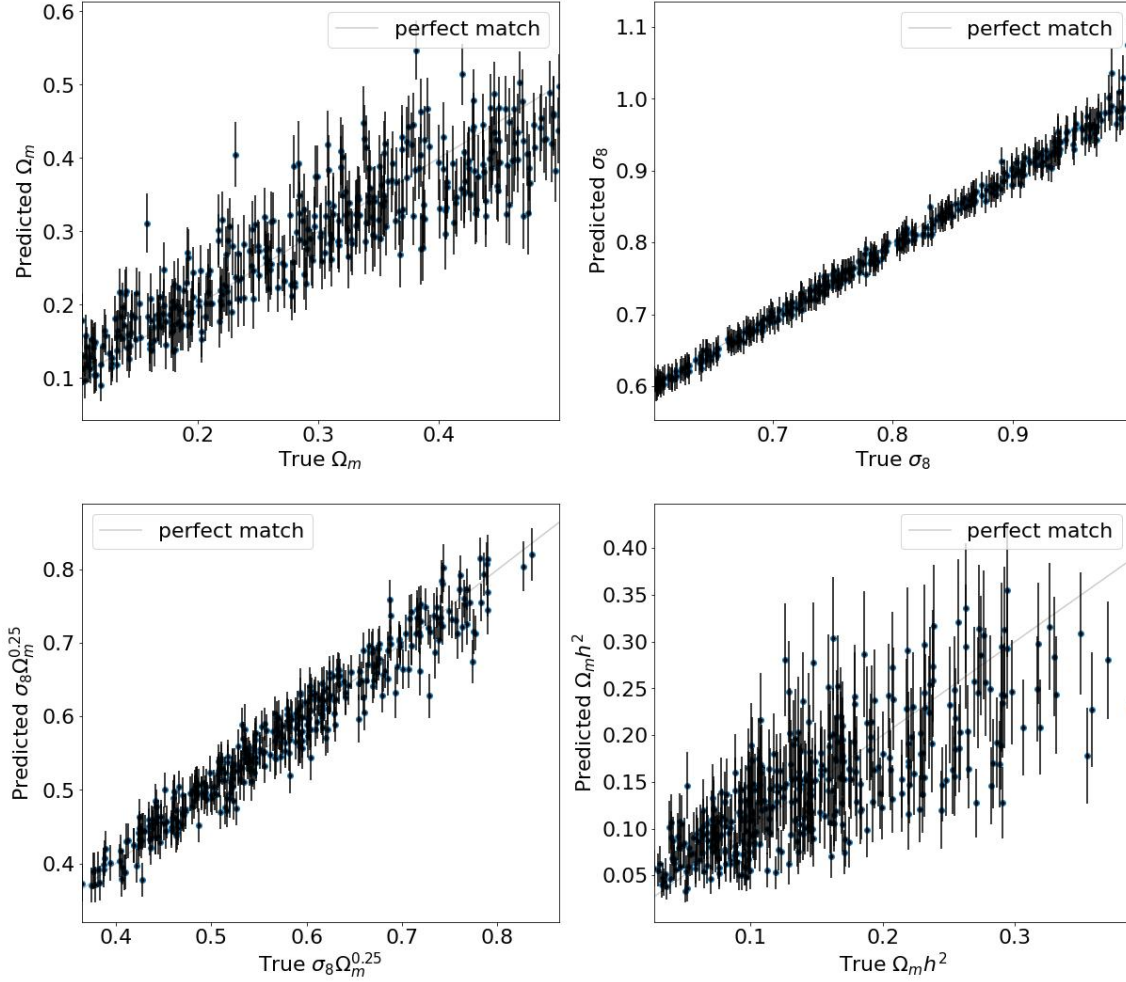


**Figure 2.** Plots of True vs Predicted values provided by the best experiment VBNNs, for  $\Omega_m$ ,  $\sigma_8$ , and some derivative parameters. Points are the mean of the predicted distributions, and error bars stand for the heteroscedastic uncertainty associated to epistemic plus aleatoric uncertainty at  $1\sigma$ .

the others we have just 3-4 of them. Next, we employed the  $\sigma$ -scaling methodology for calibrating the FlipoutBNNs predictions (31). For doing so, we optimize uniquely the loss function described in Eq. 12 where all parameters related to the BNNs were frozen, i.e., the only trainable parameter was  $s$ . After training, we got  $s \sim 0.723$ , reducing UCE only up to 10%, and the number of samples in the calibration diagrams enlarged to 4-5. This minor performance enhancement means that  $\sigma$ -scaling is not suitable to calibrate all BNNs, and alternative re-calibration techniques must be taken into account in order to build reliable intervals. At this point, we have noticed the advantages of working with methods that leading with networks already well-calibrated after the training step (17).

## 5.2 Joint analysis for Cosmological parameters

In order to show the parameter intervals and contours from the N-body simulations, we choose randomly an example from the test set with true values shown in table 3. The two-dimensional posterior distribution of the cosmological parameters are shown in figure 4 and the parameter 95% intervals are reported in table 3. We can observe that VBNNs provides considerably tighter and well constraints on all parameters

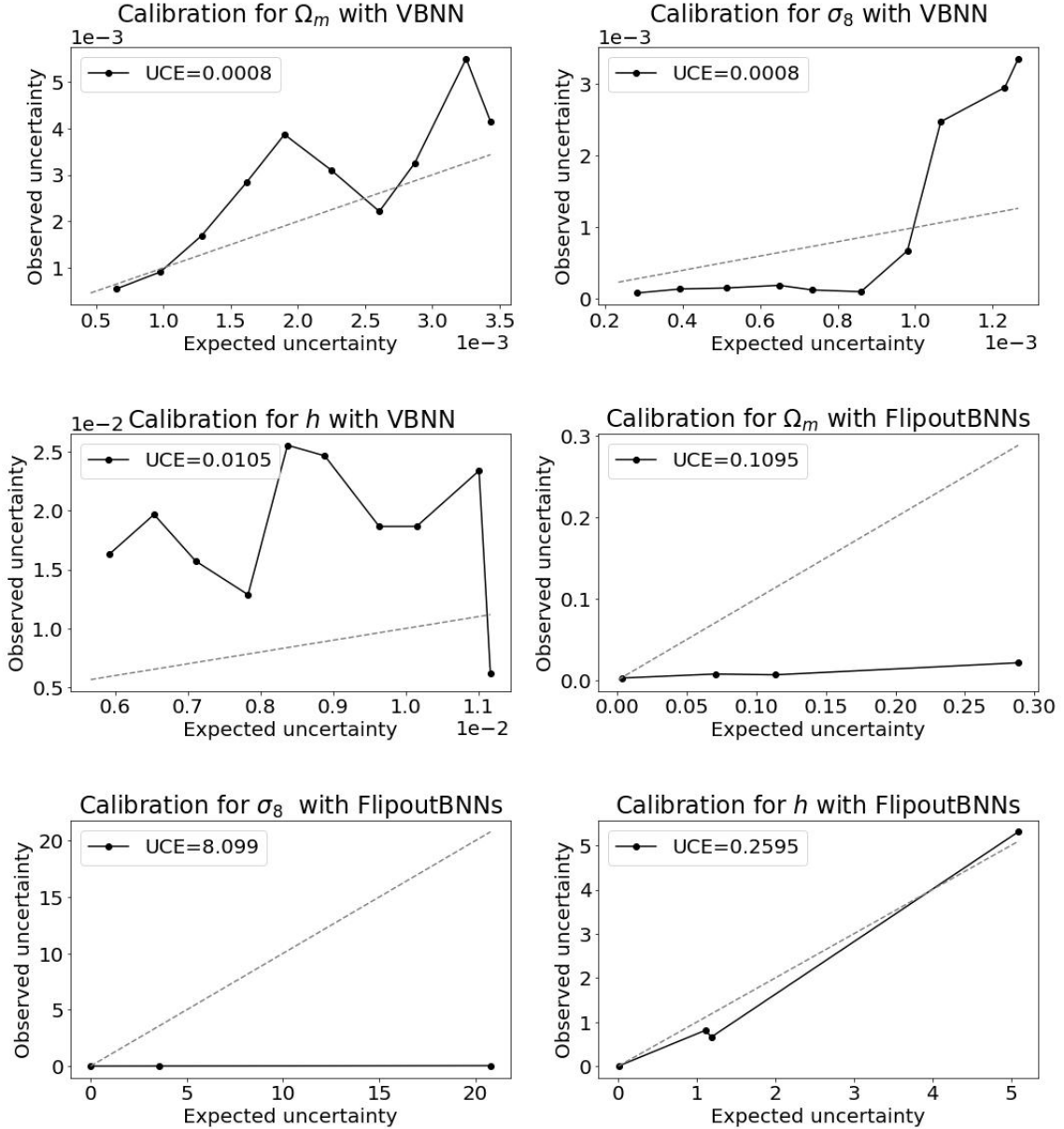


**Figure 3.** Calibration diagrams for the best experiments, VBNNs and FlipoutBNNs. The lower is the UCE value, the higher is the calibration of the model. Dashed lines stand for the perfect calibration, so, the discrepancy to this identity curve reveals miscalibration.

with respect to the sBNNs (18). Most important, this technique offers also the correlation among parameters and the measurement about how reliable the model in their predictions.

## 6 CONCLUSIONS

N-body simulations offer one of the most powerful ways to understand the initial conditions of the Universe and improve our knowledge on fundamental physics. In this paper we used QUIJOTE dataset, in order to show how convolutional DNNs capture non-Gaussian patterns without requiring a specifying the summary statistic (such as PS). Additionally, we have show how we can build probabilistic DNNs to obtain uncertainties which account for the reliability in their predictions. One of the main goals of this paper was

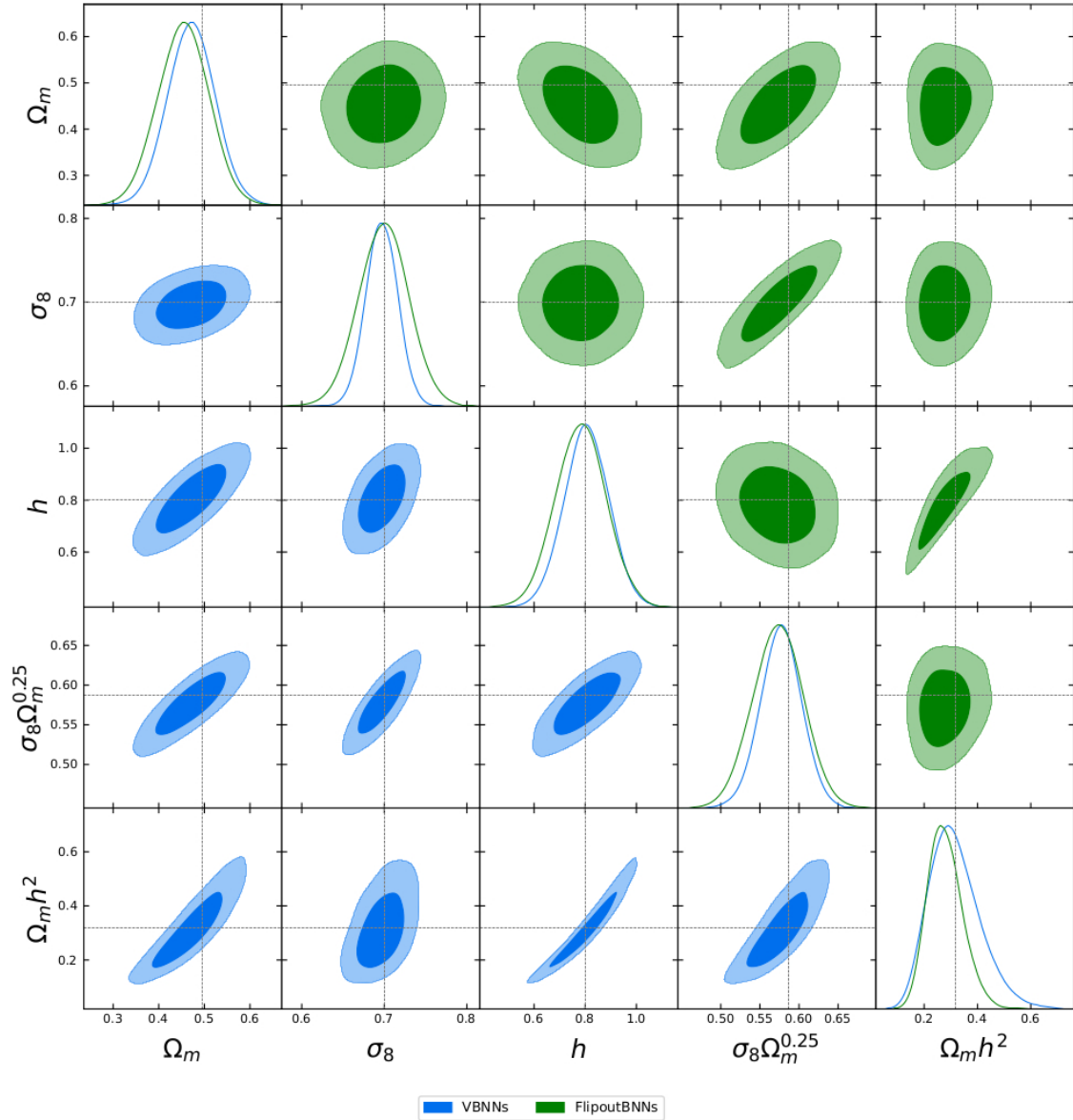


**Figure 4.** 68% and 95% parameter constraint contours from one example of Quijote test dataset using VBNNs and FlipoutBNNs. The diagonal plots are the marginalized parameter constraints, the dashed lines stand for the true values. This plot was made using Getdist (42).

also reporting how improves these BNNs when we integrate them with techniques such as a Multiplicative normalizing flows to enhance the variational posterior complexity. We found that VBNNs not only provides considerably tighter and well constraints on all cosmological parameters as we observed in figure 4, but also yields with well-calibrated estimate uncertainties as it was shown in figure 3. Nevertheless, some limitations in this research includes simple prior assumptions (mean-field approximations), lower resolution in the simulations, and absence of additional calibration techniques. These restrictions will be analysed in detail in a future paper.

Parameter	95% limits VBNNs	95% limits FlipoutBNNs	True Value
$\Omega_m$	$0.47^{+0.10}_{-0.10}$	$0.45^{+0.11}_{-0.11}$	0.495
$\sigma_8$	$0.697^{+0.038}_{-0.038}$	$0.699^{+0.059}_{-0.060}$	0.699
$h$	$0.81^{+0.17}_{-0.17}$	$0.78^{+0.20}_{-0.19}$	0.800
$\sigma_8 \Omega_m^{0.25}$	$0.577^{+0.051}_{-0.052}$	$0.573^{+0.063}_{-0.064}$	0.587
$\Omega_m h^2$	$0.31^{+0.19}_{-0.18}$	$0.573^{+0.063}_{-0.064}$	0.317

**Table 3.** Parameter 95% intervals taken from the parameter constraint contours (figure 4) from one example of Quijote test dataset using VBNN and FlipoutBNN.

## ACKNOWLEDGMENTS

This paper is based upon work supported by the Google Cloud Research Credits program with the award GCP19980904.

Leonardo Castañeda was supported by patrimonio autónomo fondo Nacional de financiamiento para la ciencia y la tecnología y la innovación Francisco José de Caldas (Minciencias Colombia) grant No 110685269447 RC-80740-465-2020 projects 69723. H. J. Hortúa acknowledges the support from créditos educación de doctorados nacionales y en el exterior- colciencias, and the grant provided by the Google Cloud Research Credits program.

## REFERENCES

- 1 .Stefano B, Kravtsov A. Cosmological simulations of galaxy clusters. *Advanced Science Letters* **4** (2011) 204–227. doi:10.1166/asl.2011.1209.
- 2 .Dodelson S. *Modern Cosmology* (Academic Press, Elsevier Science) (2003).
- 3 .Planck C, Aghanim N, Akrami Y, Ashdown M, Aumont J, Baccigalupi C, et al. Planck 2018 results. *Astronomy and Astrophysics* **641** (2020) A6. doi:10.1051/0004-6361/201833910.
- 4 .Tinker JL, Sheldon ES, Wechsler RH, Becker MR, Rozo E, Zu Y, et al. COSMOLOGICAL CONSTRAINTS FROM GALAXY CLUSTERING AND THE MASS-TO-NUMBER RATIO OF GALAXY CLUSTERS. *The Astrophysical Journal* **745** (2011) 16. doi:10.1088/0004-637x/745/1/16.
- 5 .Yusofi E, Ramzanpour MA. Cosmological constant problem and  $h_0$  tension in void-dominated cosmology (2022). doi:10.48550/ARXIV.2204.12180.
- 6 .Mesinger A, Furlanetto S, Cen R. 21cmfast: a fast, seminumerical simulation of the high-redshift 21-cm signal. *Monthly Notices of the Royal Astronomical Society* **411** (2011) 955–972. doi:10.1111/j.1365-2966.2010.17731.x.
- 7 .Hamann J, Hannestad S, Lesgourgues J, Rampf C, Wong YY. Cosmological parameters from large scale structure - geometric versus shape information. *Journal of Cosmology and Astroparticle Physics* **2010** (2010) 022–022. doi:10.1088/1475-7516/2010/07/022.
- 8 .Abdalla E, Abell’an GF, Aboubrahim A, Agnello A, Akarsu O, Akrami Y, et al. Cosmology intertwined: A review of the particle physics, astrophysics, and cosmology associated with the cosmological tensions and anomalies. *Journal of High Energy Astrophysics* (2022).
- 9 .Gillet N, Mesinger A, Greig B, Liu A, Ucci G. Deep learning from 21-cm tomography of the cosmic dawn and reionization. *Monthly Notices of the Royal Astronomical Society* **484** (2019) 282–293. doi:10.1093/mnras/stz010.
- 10 .Dvorkin C, Mishra-Sharma S, Nord B, Villar VA, Avestruz C, Bechtol K, et al. Machine learning and cosmology (2022). doi:10.48550/ARXIV.2203.08056.

- 11 .Guo C, Pleiss G, Sun Y, Weinberger KQ. On calibration of modern neural networks. *Proceedings of the 34th International Conference on Machine Learning - Volume 70 (JMLR.org)* (2017), ICML 17, 1321–1330.
- 12 .Chang DT. Bayesian neural networks: Essentials (2021). doi:10.48550/ARXIV.2106.13594.
- 13 .Ravanbakhsh S, Oliva J, Fromenteau S, Price LC, Ho S, Schneider J, et al. Estimating cosmological parameters from the dark matter distribution (2017). doi:10.48550/ARXIV.1711.02033.
- 14 .Lazanu A. Extracting cosmological parameters from n-body simulations using machine learning techniques. *Journal of Cosmology and Astroparticle Physics* **2021** (2021) 039. doi:10.1088/1475-7516/2021/09/039.
- 15 .Wang BY, Pisani A, Villaescusa-Navarro F, Wandelt BD. Machine learning cosmology from void properties (2022). doi:10.48550/ARXIV.2212.06860.
- 16 .Hortúa HJ, Volpi R, Marinelli D, Malagò L. Parameter estimation for the cosmic microwave background with bayesian neural networks. *Physical Review D* **102** (2020). doi:10.1103/physrevd.102.103509.
- 17 .Hortúa HJ, Malagò L, Volpi R. Constraining the reionization history using bayesian normalizing flows. *Machine Learning: Science and Technology* **1** (2020) 035014. doi:10.1088/2632-2153/aba6f1.
- 18 .Hortúa HJ. Constraining cosmological parameters from n-body simulations with bayesian neural networks (2021). doi:10.48550/ARXIV.2112.11865.
- 19 .Mancarella M, Kennedy J, Bose B, Lombriser L. Seeking new physics in cosmology with bayesian neural networks: Dark energy and modified gravity. *Phys. Rev. D* **105** (2022) 023531. doi:10.1103/PhysRevD.105.023531.
- 20 .List F, Rodd NL, Lewis GF, Bhat I. Galactic center excess in a new light: Disentangling the gamma-ray sky with bayesian graph convolutional neural networks. *Physical Review Letters* **125** (2020). doi:10.1103/physrevlett.125.241102.
- 21 .Wagner-Carena S, Park JW, Birrer S, Marshall PJ, Roodman A, Wechsler RH. Hierarchical inference with bayesian neural networks: An application to strong gravitational lensing. *The Astrophysical Journal* **909** (2021) 187. doi:10.3847/1538-4357/abdf59.
- 22 .Graves A, editor. *Practical Variational Inference for Neural Networks*, vol. 24 (Curran Associates, Inc.) (2011).
- 23 .Charnock T, Perreault-Levasseur L, Lanusse F. Bayesian neural networks (2020). doi:10.48550/ARXIV.2006.01490.
- 24 .Villaescusa-Navarro F, Hahn C, Massara E, Banerjee A, Delgado AM, Ramanah DK, et al. The quijote simulations. *The Astrophysical Journal Supplement Series* **250** (2020) 2. doi:10.3847/1538-4365/ab9d82.
- 25 .Abdar M, Pourpanah F, Hussain S, Rezazadegan D, Liu L, Ghavamzadeh M, et al. A review of uncertainty quantification in deep learning: Techniques, applications and challenges. *Information Fusion* **76** (2021) 243–297. doi:10.1016/j.inffus.2021.05.008.
- 26 .Gal Y. *Uncertainty in Deep Learning*. Ph.D. thesis, University of Cambridge (2016).
- 27 .Wen Y, Vicol P, Ba J, Tran D, Grosse R. Flipout: Efficient pseudo-independent weight perturbations on mini-batches (2018). doi:10.48550/ARXIV.1803.04386.
- 28 .Kiureghian AD, Ditlevsen O. Aleatory or epistemic? does it matter? *Structural Safety* **31** (2009) 105 – 112. doi:https://doi.org/10.1016/j.strusafe.2008.06.020. Risk Acceptance and Risk Communication.
- 29 .Kendall A, Gal Y. What uncertainties do we need in bayesian deep learning for computer vision? (2017).
- 30 .Kwon Y, Won JH, Joon Kim B, Paik M. *Ininternational conference on medical imaging with deep learning* (2018) 13.

- 31 .Laves MH, Ihler S, Fast JF, Kahrs LA, Ortmaier T. Well-calibrated regression uncertainty in medical imaging with deep learning. *Medical Imaging with Deep Learning* (2020).
- 32 .Louizos C, Welling M. Multiplicative normalizing flows for variational bayesian neural networks. *Proceedings of the 34th International Conference on Machine Learning - Volume 70* (JMLR.org) (2017), ICML'17, 2218–2227.
- 33 .Ranganath R, Tran D, Blei DM. Hierarchical variational models. *Proceedings of the 33rd International Conference on International Conference on Machine Learning - Volume 48* (JMLR.org) (2016), ICML'16, 2568–2577.
- 34 .Touati A, Satija H, Romoff J, Pineau J, Vincent P. Randomized value functions via multiplicative normalizing flows (2018). doi:10.48550/ARXIV.1806.02315.
- 35 .Dinh L, Sohl-Dickstein J, Bengio S. Density estimation using real NVP. *International Conference on Learning Representations* (2017).
- 36 .Springel V. The cosmological simulation code gadget-2. *Monthly Notices of the Royal Astronomical Society* **364** (2005) 1105–1134. doi:10.1111/j.1365-2966.2005.09655.x.
- 37 .Scoccimarro R. Transients from initial conditions: a perturbative analysis. *Monthly Notices of the Royal Astronomical Society* **299** (1998) 1097–1118. doi:10.1046/j.1365-8711.1998.01845.x.
- 38 .Abadi M, Agarwal A, Barham P, Brevdo E, Chen Z, Citro C, et al. TensorFlow: Large-scale machine learning on heterogeneous systems (2015). Software available from tensorflow.org.
- 39 .Solovyev R, Kalinin AA, Gabruseva T. 3d convolutional neural networks for stalled brain capillary detection. *Computers in Biology and Medicine* **141** (2022) 105089. doi:10.1016/j.combiomed.2021.105089.
- 40 .Kingma DP, Ba J. Adam: A method for stochastic optimization (2014). doi:10.48550/ARXIV.1412.6980.
- 41 .Sønderby CK, Raiko T, Maaløe L, Sønderby SK, Winther O. Ladder variational autoencoders. *Proceedings of the 30th International Conference on Neural Information Processing Systems* (Red Hook, NY, USA: Curran Associates Inc.) (2016), NIPS'16, 3745–3753.
- 42 .Lewis A. GetDist: a Python package for analysing Monte Carlo samples (2019).